AIAA JOURNAL
Vol. 34, No. 3, March 1996

Complete Three-Dimensional Multiparameter Mapping of a Supersonic Ramp Fuel Injector Flowfield

James M. Donohue* and James C. McDaniel Jr.†
University of Virginia, Charlottesville, Virginia 22903

Planar laser-induced iodine fluorescence is used to map out the nonreacting mixing flowfield of an unswept ramp fuel injector using air injected at Mach 2.0 into a Mach 2.9 freestream. A fully automated test setup is used to measure time-averaged pressure, temperature, velocity, and injectant mole fraction on 21 crossflow planes and 7 axial planes. The measurement uncertainties are 5–8% for temperature, 4–10% for pressure, 10–20 m/s for velocity, and 2–3% for injectant mole fraction depending on the thermodynamic conditions. The measurements allow any desired gasdynamic quantity to be determined on a three-dimensional grid that spans the entire wind-tunnel test section. The experimental data set is comparable to the completeness of results normally available only from a computational fluid dynamics simulation. Results showing detailed flow features on specific planes, as well as overall quantities, such as global conservation checks, mixing performance, and flowfield losses, are presented. Mass, momentum, and energy flux, determined at the crossflow plane locations of the data set, show about a 2% standard deviation. The results are compared to a simulation using a three-dimensional Navier–Stokes solver. Agreement is reasonable with the exception of measurements in regions very close to walls, where the intensity of scattered light is high or where optical access is limited. The ability to generate extensive data sets, such as the one presented here, demonstrates that the planar laser-induced iodine fluorescence technique can be used 1) to generate detailed test cases for the validation of computational fluid dynamics codes and 2) as an alternative to computational fluid dynamics for performing design studies and performance evaluation in complex compressible flows.

Introduction

THERE has been considerable interest in the development of enhanced fuel/air mixing schemes for supersonic combusting flowfields. Uniform and rapid mixing allows for shorter combustor lengths, higher combustion efficiencies, and better engine operation. Of the various supersonic mixing enhancement schemes proposed, wall-mounted ramp injectors have been strongly considered because they generate strong mixing vortices and introduce relatively low flowfield losses.[1] Several studies specifically related to the three-dimensional mixing flowfield of ramp injectors have been reported previously.[2–5] The axial injection configuration used with ramps has two important advantages over transverse injection configurations: 1) additional thrust is generated by injecting fuel in the downstream direction and 2) the undesirable bow shock formed when fuel is injected transversely into a supersonic free stream is avoided. The design of such injection schemes relies on the understanding of extremely complex flowfields with features such as turbulent mixing, combustion reactions, strong three dimensionality, compressibility effects, boundary layers, and flow separations.

Of the experimental techniques available for studying supersonic flowfields, laser diagnostic techniques are particularly attractive. They are inherently nonintrusive and have the ability to generate data with excellent spatial resolution. The applicability of using planar laser-induced iodine fluorescence (PLIIF) techniques for investigations of supersonic fuel injector flowfields has been well demonstrated in a recent study of swept ramp injection[6] and in a study of staged transverse injection behind a rearward facing step.[7,8] In these studies, excellent agreement was seen in comparisons between the iodine fluorescence measurements and numerical simulations of the flowfields using the SPARK Navier–Stokes solver.[9,10] The ability of PLIIF to measure all relevant flowfield parameters on multiple planes, with various orientations, makes it a unique tool for visualizing and quantifying the important three-dimensional phenomena present in these high-speed compressible flows. The objective of the unswept ramp test case presented here is to make available an experimental data set with sufficient completeness and accuracy for present and future computational fluid dynamics (CFD) validation and for measurement consistency evaluation using global conservation principles.

Presented as Paper 95-0519 at the AIAA 33rd Aerospace Sciences Meeting, Reno, NV, Jan. 9–12, 1995; received Jan. 20, 1995; revision received July 3, 1995; accepted for publication July 27, 1995.

*Research Associate, Department of Mechanical, Aerospace, and Nuclear Engineering; currently Assistant Professor, Department of Mechanical Engineering, Santa Clara University, Santa Clara, CA 95053. Member AIAA.

†Professor, Department of Mechanical, Aerospace, and Nuclear Engineering. Member AIAA.

Experimental Approach

Test Facility and Injector Model

The test facility is a continuous-flow supersonic wind tunnel containing a compressed air supply, an iodine seeding chamber, a two-dimensional Laval nozzle, a test section, and exhaust ducts. Iodine is an excellent candidate seed molecule for LIF measurements in air flows. It has adequate vapor pressure at room temperature to allow for easy flowfield seeding. In the seeding arrangement used here, the wind-tunnel air is simply passed over several trays of iodine beads. The residence time of the air inside the seeding chamber is long enough that the seeding level approaches the iodine vapor pressure. Iodine exhibits a strong fluorescence spectrum with numerous absorption transitions in the visible range, making it accessible to many different types of lasers. It is highly corrosive and is somewhat toxic, however, so that it requires careful handling and a wind-tunnel facility specifically designed for iodine compatibility. The wind-tunnel air is filtered and dried before it enters the test facility, which helps to reduce iodine condensation and corrosion.

The geometry of the wind-tunnel test section and the unswept ramp injector tested are presented in Fig. 1. The ramp has a 10-deg compression angle and a base height of 7.49 mm. All dimensions shown are nondimensionalized with this base height H. The base has an aspect ratio, height to width, of 1.62. Air is injected from the face of the ramp base and is inclined at a 20-deg angle to the horizontal. The ramp sits in a rectangular duct with a cross section of $2.54H$ by $4.07H$. The test section has a constant area for approximately 14.4 ramp heights downstream of the ramp up to the tunnel's second throat. The nominal inlet Mach number from the supersonic nozzle is 2.9. The injector orifice is contoured to give air injected at Mach 2.0. Inlet stagnation conditions for the freestream air are 300 K and 690 kPa. Stagnation conditions for the jet, measured just upstream of the injector block, are 302 K and 680 kPa. The coordinate system

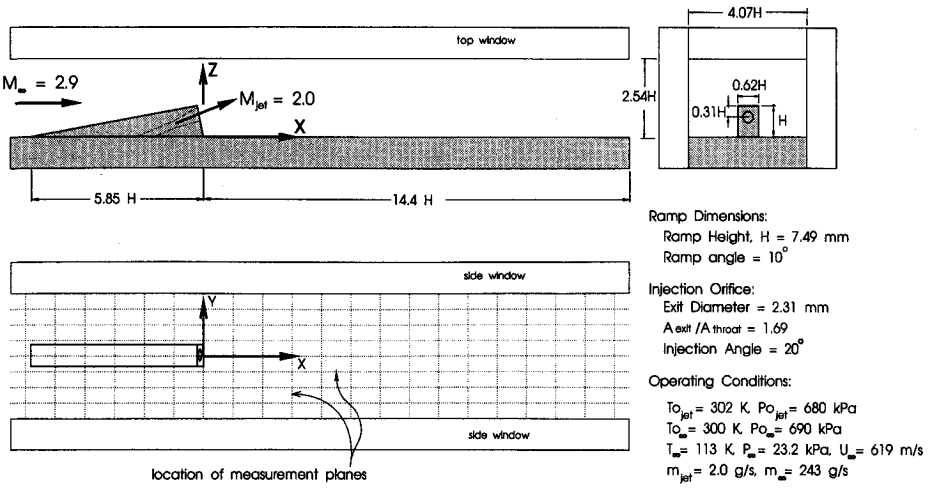

Fig. 1 Test section geometry and operating conditions.

is shown in Fig. 1 with x the streamwise or axial direction, y the spanwise or lateral direction, and z the vertical direction measured normal to the injector wall. The origin is located on the bottom wall at the base of the ramp.

The location of planes where measurements were taken, oriented both axially and in the crossflow direction, is indicated in Fig. 1 as dotted lines. Axial plane measurements were taken at 7 locations equally spaced from $Y/H = -1.5H$ to $+1.5H$. The axial plane measurements were made using laser sheets from two separate regions and patched together at $X/H = 6$. This was done to avoid spreading the laser sheet across the entire length of the tunnel that would cause an excessive decrease in fluorescence intensity levels. Crossflow planes are taken at 21 equally spaced locations starting from before the ramp leading edge, at $X/H = -6$, to the end of the test section, at $X/H = 14$. Note that two laser sheet directions are needed for each measurement plane to capture the two velocity components in the plane. The sheet directions used were chosen to capture as much of the flowfield as possible, but some small regions close to walls could not be accessed with both sheets. Also, because the images are being collected through the side window for both the axial and crossflow plane measurements, in some images a small region of the flowfield is hidden behind the ramp, out of view of the camera used to collect the images. This leaves some small gaps in the measurement data set. By using symmetry arguments, the missing information could be filled in with data from the opposite side of the ramp, if completion of the data set in this region is desired.

PLIIF Multiparameter Measurement Technique

The ability to make multiparameter flowfield measurements with PLIIF relies on the fact that the measured fluorescence signal levels and the shape of the fluorescence spectrum depend strongly on the gasdynamic parameters of the flowfield. In the technique used here, a small region of the iodine absorption spectrum is measured with an argon ion laser, operated narrowband and tuned across two spectral lines accessible at the 514.5-nm argon line. Flowfield parameters are determined by comparing the measured spectra to the spectra predicted by a theoretical model. Iodine fluorescence modeling has been the subject of research for many years and details of the model used here have been previously reported.[11–14] The fluorescence signal S_f can be represented as a complicated function of the pressure P, temperature T, velocity component in the beam direction u, and laser frequency ν, and is proportional to the laser intensity I, and to the number density of iodine present in the flow N_{I_2}:

$$S_f = f(P, T, u, \nu) I N_{I_2} \tag{1}$$

The fluorescence signal has the advantage of being sensitive to all flow parameters of interest, but has the disadvantage of being a strongly coupled function of the parameters, so that specially developed approaches must be used to measure each parameter individually. The shape of the fluorescence spectrum is used to determine the flowfield pressure and temperature. Figure 2 shows measured and modeled iodine spectra at three typical flowfield conditions. The relative peak heights of the two lines are sensitive to temperature due to the different ground state Boltzmann population dependence of the transitions that make up these lines. The width, or broadening, of the spectra is strongly sensitive to pressure due to collisional effects. The center spectra in Fig. 2 illustrates the velocity measurement technique, showing a Doppler shift of the measured vs modeled spectra due to the flowfield velocity having a component in the laser beam direction. The fact that the signal level is directly proportional to iodine number density is utilized for injectant mole fraction measurements.

To make accurate, quantitative, planar measurements, considerable attention must be paid to the illumination optics and image collection system used. A 200-μm-thick laser sheet is created from the laser beam using a cylindrical lens and a spherical lens. A liquid-nitrogen cooled charge-coupled device (CCD) camera is used to image the resulting iodine fluorescence. The Photometrics CH210 camera is used because of its high degree of linearity, its low dark current noise levels, and the high resolution it provides (516 by 516 pixels with 14-bit intensity levels). Exposure times were typically about 20 s. To position the laser sheet at the desired location, the optics are mounted on a computer-controlled translation stage. All lenses and mirrors and the camera are mounted on the translation stage so that the alignment of the optics is maintained as the sheet is scanned throughout the flowfield. A portion of the laser beam is split off and used to monitor the laser's power and frequency. The improved PLIIF technique, used for this study, gives more accurate measurements and allows for full automation of the measurement procedures so that complete flowfield mapping tests can now be performed. The need for automation is clear when considering the quantity of data and postprocessing required. For 21 spatial flowfield locations and two velocity components in each plane, approximately 2100 images are acquired. This corresponds to about 1 Gbyte of raw data to be stored and 10×10^6 nonlinear least-square curvefits to be performed.

Experimental uncertainties are due to factors such as inaccuracies in the iodine fluorescence modeling, shot noise, and variations in the inlet stagnation conditions. Turbulent fluctuations in the flowfield contribute some additional uncertainty since the fluorescence signal level is a nonlinear function of the properties. Except in very high-turbulence intensity regions, close to walls and in recirculation regions, the effect of fluctuations is expected to be negligible. Images are corrected for laser power variations by dividing each image by the laser power measured during the exposure. To correct for variations in the iodine seeding level the signal from the beam of a second argon ion laser, operated broadband and directed inside the flowfield at the edge of the camera's field of view, is used. The overall experimental uncertainties depend strongly on the local thermodynamic conditions. For the flowfield conditions studied here, ranges of uncertainties are 5–8% for temperature, 4–10% for

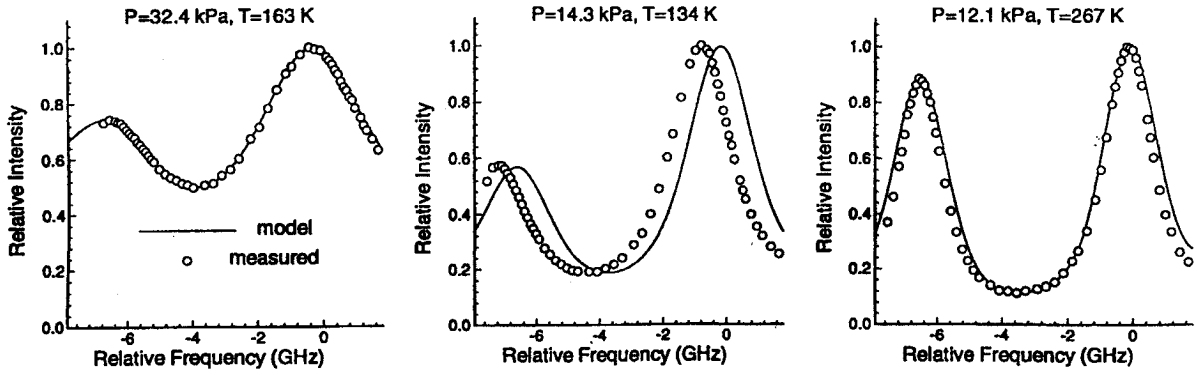

Fig. 2 Measured and modeled iodine fluorescence spectra, showing the variation with thermodynamic conditions; center plot indicates a Doppler shift due to a component of velocity in the laser beam direction.

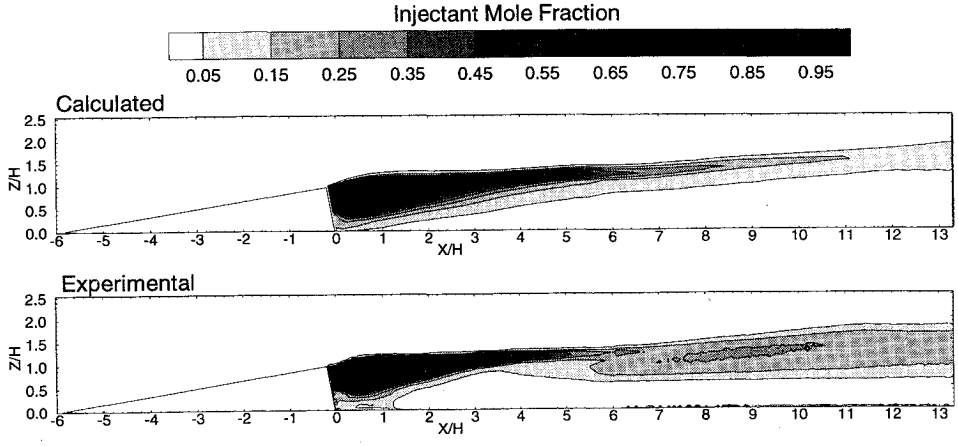

Fig. 3 Centerplane injectant mole fraction distribution.

pressure, 10–20 m/s for velocity, and 2–3% for injectant mole fraction. Uncertainties are higher in regions close to walls mostly due to high levels of scattered light from tunnel walls. A more detailed presentation of the measurement techniques, test setup, and uncertainty analysis appear elsewhere.[15,16]

Numerical Approach

For comparison to the PLIIF measurements, a numerical simulation of the flowfield was performed using the SPARK CFD code. SPARK, originally developed by Drummond[9] and extended to three-dimensions by Carpenter,[10] utilizes a finite difference discretization of the full Reynolds-averaged Navier–Stokes equations. It has the ability to simulate finite rate chemistry for combusting flows, a feature that was turned off for the nonreacting flowfield of interest here. It uses a MacCormack predictor–corrector scheme and high-order compact differencing giving fourth-order accuracy at steady state. Local time stepping is used to accelerate convergence to the steady-state solution. The simulation was performed on only one-half of the symmetric flowfield. The grid used was generated to fit all solid boundaries smoothly and was compressed at the location of boundary layers and shear layers to capture the high gradients in these regions. Slip boundary conditions where used on the tunnel side walls to reduce the number of grid points needed and save computational requirements. The grid contained approximately 200,000 points with 50 by 60 points in the crossflow planes. Algebraic models were used to simulate the mixing due to turbulence. The Baldwin–Lomax model was used along walls and a mixing length model was used to model the jet turbulence.[6,16]

Results

Example Planar Results

Several planes of data are presented herein, along with results from the SPARK calculation as examples of the full data set. The pressure, temperature, and velocity are all given in nondimensional form, with the conditions at the inlet to the test section used as the reference conditions. The range of the data shown in the axial planes is from $X/H = -6$–13.2 and $Z/H = 0$–2.5. Crossflow plane results are shown from $Y/H = -1.4$ to $+1.4$ and $Z/H = 0$–2. Injectant mole fraction distribution at the center axial plane is shown in Fig. 3. Penetration of the plume into the freestream is similar in the measured and calculated results. A better view of the structure of the plume is presented in the crossflow results. Crossflow planes at $X/H = 1$, 5, and 10 are shown in Fig. 4. The plume shows the characteristic two-lobed kidney shape due to the pair of counter-rotating vortices formed by the ramp. It is interesting to compare the unswept ramp results here to measurements made in the same wind tunnel on a swept ramp injector.[2] There is significantly more spreading and turning of the initial plume in the swept ramp case, as expected, due to the stronger mixing vortices formed. This comparison is complicated by the fact that several parameters, such as the injector orifice and base geometry, are similar but not exactly the same for the two cases. Comparison between the SPARK calculation and the experimental results shows good agreement in terms of contour levels at each downstream location. The shapes of the plume cross sections are somewhat different due to damping of the mixing vortices as they are convected downstream in the calculation. Asymmetry of the experimental plume, particularly noticeable at the $X/H = 5$ location, comes about due to different strength vortices formed on either side of the ramp. Careful inspection of the Laval nozzle showed that there is a slight but measurable asymmetry in the nozzle geometry so that the flow exiting the nozzle is most likely the cause of the asymmetry seen.

Figure 5 shows crossflow velocities at $X/H = -4$, 1, 5, and 10. The $X/H = -4$ plane cuts through the ramp at a location about $\frac{1}{3}$ of its length downstream of the ramp leading edge. The location of the ramp shock shows up clearly in the crossflow velocity components along a border around the ramp. The shock formed by the unswept ramp is strongly curved and three dimensional. The initial formation of streamwise vorticity at the sides of the ramp is also clearly seen. There is evidence of a weak planar wave along a line tangent to the top of the curved ramp shock in the measured plane at $X/H = -4$. This is caused by a slight discontinuity in the tunnel wall where the

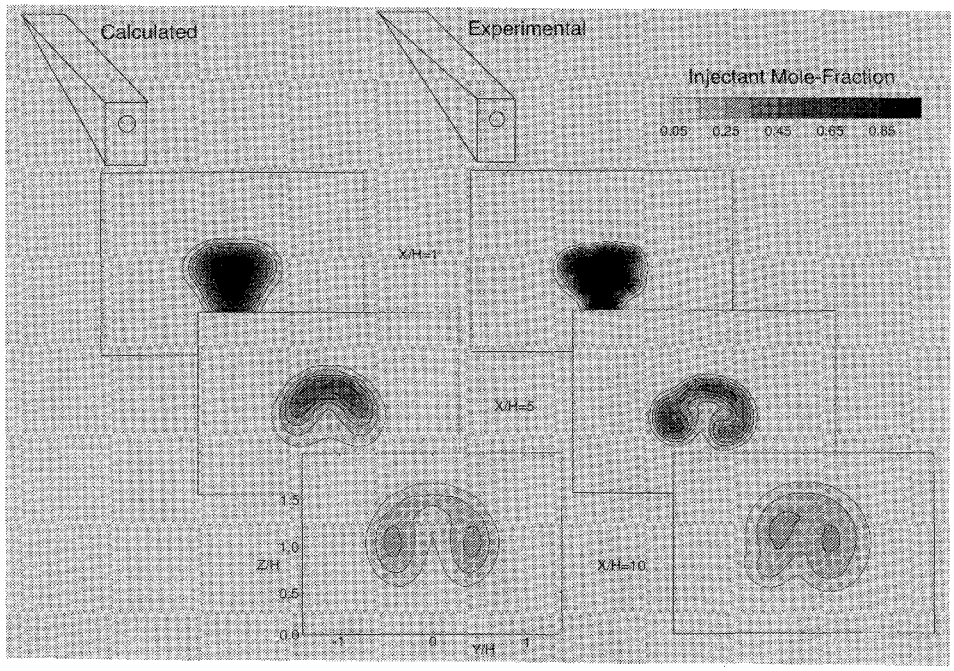

Fig. 4 Crossflow plane distributions of injectant mole fraction.

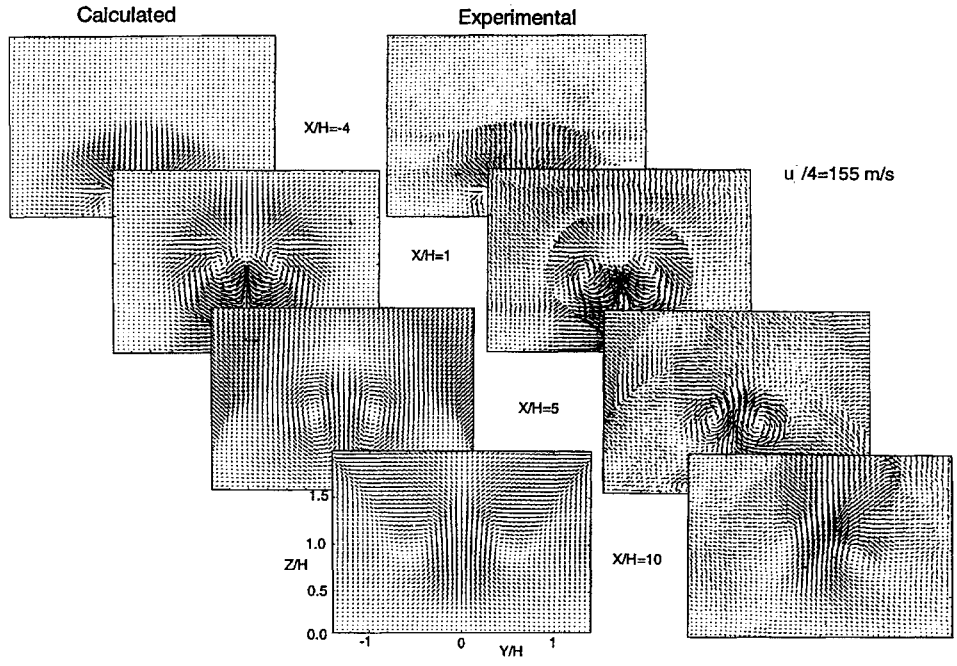

Fig. 5 Crossflow velocities.

nozzle block meets the injector. The $X/H = 1$ plane shows a slice through the conical shock formed near the ramp face where the jet diverts the freestream. The Mach disk of the jet is located almost exactly at $X/H = 1$, so that velocity vectors inside the plume show a strong focusing toward the jet core. At the two planes farther downstream, asymmetry in the crossflow velocities is more apparent. The ramp-generated vortex on the right side is consistently stronger in all of the crossflow planes. Notice that the mole fraction contours far downstream are not strongly asymmetric. This indicates that at locations far from the injection point turbulence begins to dominate the mixing process. Shock locations apparent in the velocity plots become more asymmetric with downstream distance. This is expected as shocks reflecting from the tunnel walls become more complex and distorted each time they reflect and interact. Weaker mixing vortices are seen in the calculated velocity field due to numerical damping in the vortex cores as already discussed. Significant differences in the calculated and experimental shock wave pattern are seen at the far downstream location. These differences can be attributed to inaccuracies in the boundary-layer turbulence modeling and the use of slip boundary conditions in the calculations that are unable to correctly capture the complicated shock reflections occurring on the side walls and corners of the test section.

The crossflow temperature results, presented in Fig. 6, show that the bottom wall boundary layer and jet plume size in the experimental and calculated results are in good agreement. Differences in the shape of the experimental and calculated plume, again due to dampened mixing vortices, are consistent with the injectant mole fraction and velocity results.

Figure 7 shows velocity profiles at the centerplane of the flowfield. This is one of the seven axial planes that were measured and used to determine streamwise velocity components so that flux quantities could be determined from the data. The results show every 14th

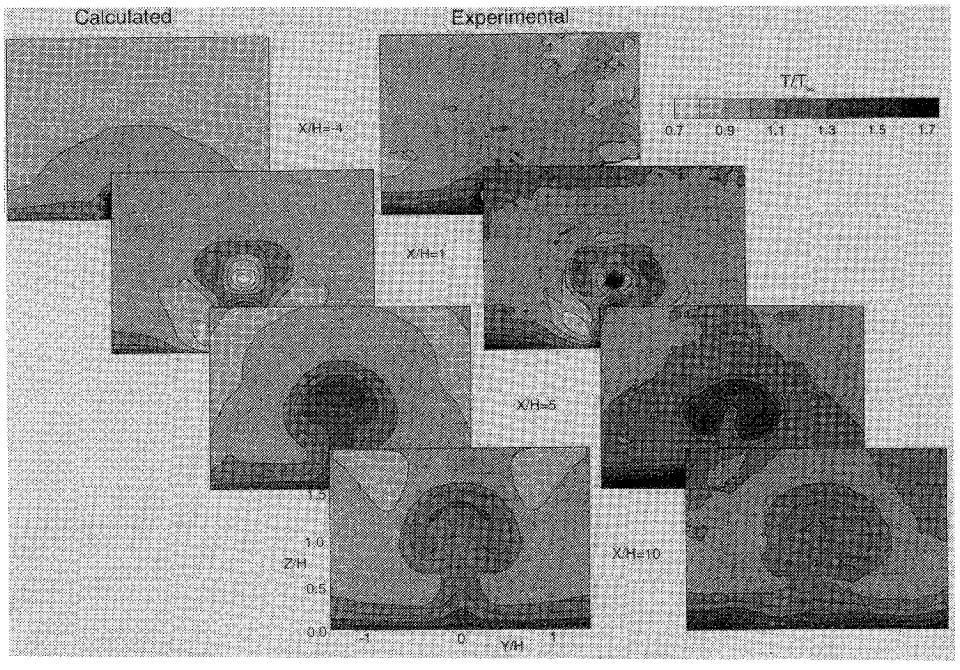

Fig. 6 Crossflow plane distributions of temperature.

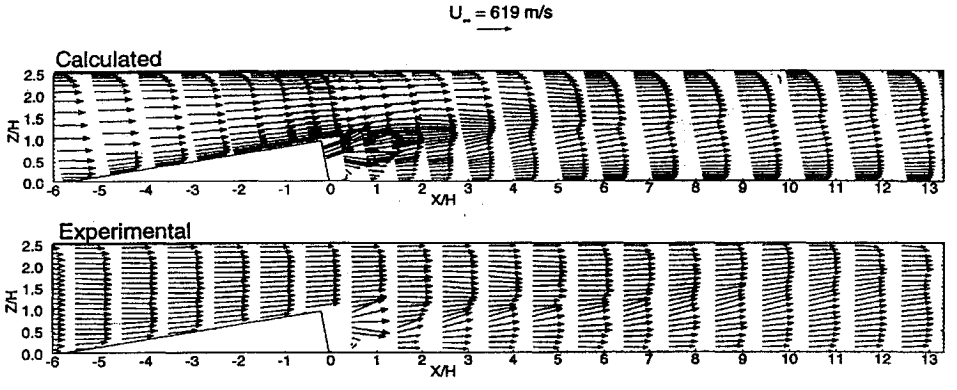

Fig. 7 Centerplane velocity profiles.

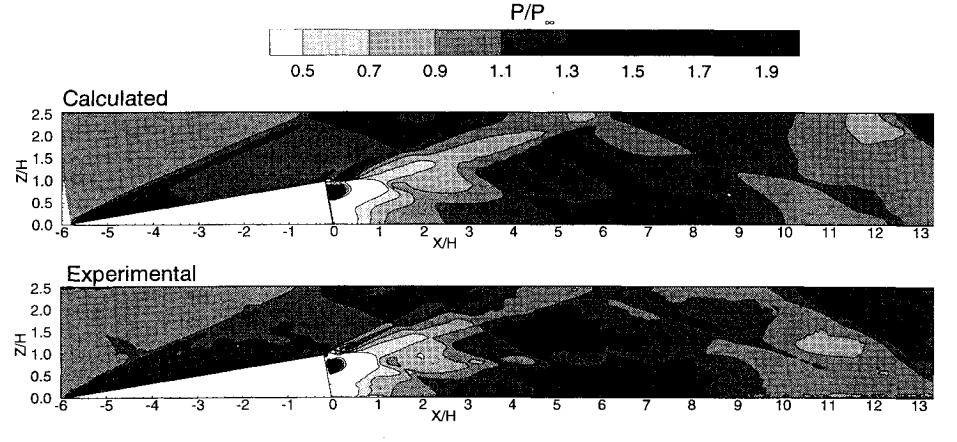

Fig. 8 Centerplane pressure distribution.

measured vector in the axial direction and every 2nd vector in the vertical direction. The calculated results are presented along lines of the numerical grid that are slanted 10 deg to match the angle of the ramp face. The measured and calculated velocities are in agreement above the ramp and in the jet plume, but the boundary layer along the lower wall shows significant differences. The pressure results at this same centerplane location are shown in Fig. 8. The pressure distribution along the bottom wall is controlled by the complex pattern of shocks reflecting from all four walls. The experimental results show shock structures similar to those seen in the calculations but, in general, the shocks in the experiments are propagating at slightly steeper angles, generating higher pressure gradients. The wall pressure distribution extracted from the data in Fig. 8 and from wall pressure taps along the tunnel centerline is shown in Fig. 9. Although the PLIIF results are

least accurate near walls, due to scattered laser light, the agreement between the pressure taps and the PLIIF results is within about 10%. The calculated results, also shown in Fig. 9, indicate two individual pressure peaks caused by shock reflections. In the experimental results these waves have coalesced, forming a single, stronger shock reflection that reaches the bottom wall earlier.

One-Dimensional Global Results Extracted from Full Data Set

Since all fundamental properties are measured on a very extensive grid, it is possible to evaluate global conservation parameters of the flowfield. The streamwise velocity component is needed to find any flux quantity through the crossflow planes. This component is interpolated from the axial plane measurements, where the streamwise velocity is measured. Note that since only 7 axial plane locations, from $-1.5H$ to $+1.5H$, are available, the crossflow data outside of $\pm 1.5H$ is not used to calculate the global quantities presented in this section. The streamwise velocity interpolation is less inaccurate close to the injectant jet where lateral gradients are very large. All information is not available on the crossflow planes upstream of the ramp due to the viewing angle used to collect the images, so the results presented will be restricted to planes downstream of the ramp base. Also, the measurements made very close to walls are less accurate so that regions within 1 mm from the upper and lower walls in the planes are excluded from the results that follow; thus, boundary-layer effects, such as heat transfer and frictional losses, are not captured.

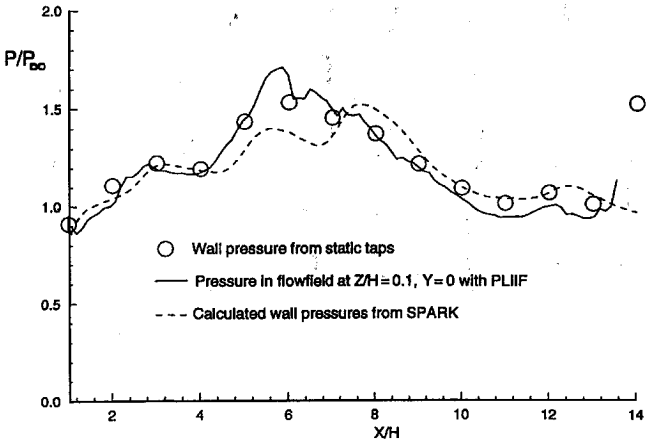

Fig. 9 Centerline wall pressures from PLIIF, wall pressure taps, and the SPARK calculation.

The values of integrated flux of mass, momentum, and energy on crossflow planes from $X/H = 1$–13 are extracted from both the measurements and the numerical simulations and are shown in Fig. 10. The plane at $X/H = 0$ is excluded because of the inaccuracies in determining velocity very close to the ramp face. The plane at $X/H = 14$ is excluded because streamwise velocity could not be determined at this location with the axial plane laser sheets used. Note that the expressions used for the momentum and energy fluxes, shown on the figure, are estimates that consider dissipation and diffusion processes negligible. The calculated values are very constant over the range shown, indicating a converged solution with deviation less than 0.5% in all three flux quantities over the domain. About a 2% variation is seen in the measured values of all three flux quantities. These results demonstrate the level of consistency and accuracy possible with the PLIIF measurement technique.

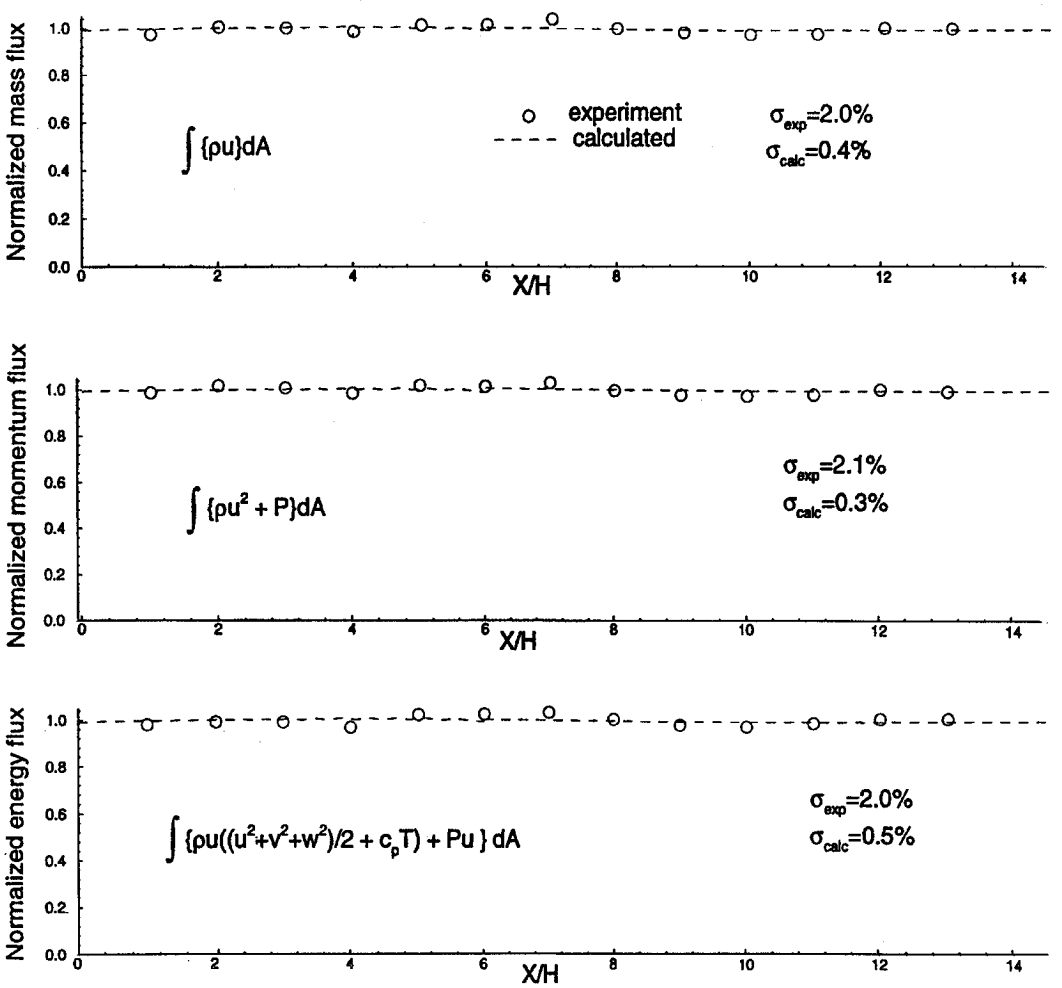

Fig. 10 Experimental and numerical evaluation of mass, momentum, and energy flux vs position downstream of the base of the ramp.

Figure 11 shows some commonly used indicators of mixing performance plotted vs downstream distance. The top plot shows the maximum value of mole fraction occurring on each crossflow plane. Decrease in the maximum level is a strong indicator of the level of mixing that has occurred and is relatively easy to measure since it requires only crossflow measurements of the mole fraction. The agreement between the calculation and the experiment at regions far downstream is within 2%. This indicates that the turbulence model employed in the numerical simulation is performing acceptably in predicting the mixing. There is a region in the measurements at around $X/H = 5$–7 where the value of χ_{max} remains at almost constant value. This unexpected trend, not seen in the calculated results, was also seen in previous measurements for unswept ramps with base aspect ratios of 1.0 and 2.0 (Ref. 17).

The middle plot of Fig. 11 shows the fraction of the crossflow plane area where the mole fraction falls between the 2% and 30% contour lines, sometimes called the percent mixed. This measure accounts for the fact that both lean and rich fuel concentrations can be outside of combustibility limits. The percent mixed measure also allows more for information about the overall shape and distribution of the mole fraction levels, rather than depending on the level at a single location. The percent mixed must increase to a maximum level and then decrease as the plume becomes more diffuse. The calculated values are higher than experimental values in the near-field region by about 3% but then fall off and are lower at downstream locations by as much as 5%. The maximum values in the two curves differ by about 1.2%. The maximum in the experimental curve occurs two ramp heights earlier than in the calculation.

The bottom plot of Fig. 11 shows the axial variation of mixing efficiency as defined by Rogers.[18] The mixing efficiency is flux based, so that unlike the other two measures discussed, it cannot be extracted from mole fraction data alone. It has been used by designers to compare fuel injection schemes simulated with CFD codes, but usually cannot be evaluated from experimental data. The rigorous definition is given in detail in Ref. 18 and will be summarized here. Mixing efficiency is an integral parameter that gives the fraction of fuel that has been mixed so that it can react to the extent of the locally available oxygen. For an overall fuel lean mixture it is represented mathematically as

$$\eta_m = \int \rho u Y_{rx} \frac{dA}{\dot{m}_f} \tag{2}$$

where

$$Y_{rx} \equiv Y_f \quad \text{if} \quad \phi \leq 1 \quad \text{or} \quad Y_{rx} \equiv f_{st}(1 - Y_f) \quad \text{if} \quad \phi > 1$$

where ϕ is the local fuel equivalence ratio, Y_f the fuel mass fraction, f_{st} the stoichiometric fuel/air ratio, and $\dot{m}_f$ is the overall fuel mass flow rate. The definition was originally formulated for hydrogen/air mixing where the stoichiometric mass fraction can be used as the reference level of mixedness. For a case with air injected into air, as is done here, the reference level used is somewhat arbitrary since a stoichiometric condition is not defined. For the results shown, the experimental value of χ_{max} found at the exit of the test section is chosen as the reference level. The mixing efficiency is then an indicator of the level of mixing attained at each axial location, compared to the level reached by the end of the experimental test section. The calculated and experimental curves agree within 15% along the entire length, with much better agreement at the downstream end where the flux measurements are expected to be more accurate. The important result here is that there is sufficient experimental data available to evaluate the many different measures of mixing that are routinely available from three-dimensional numerical simulations and that the experimental and numerical results are in reasonable agreement.

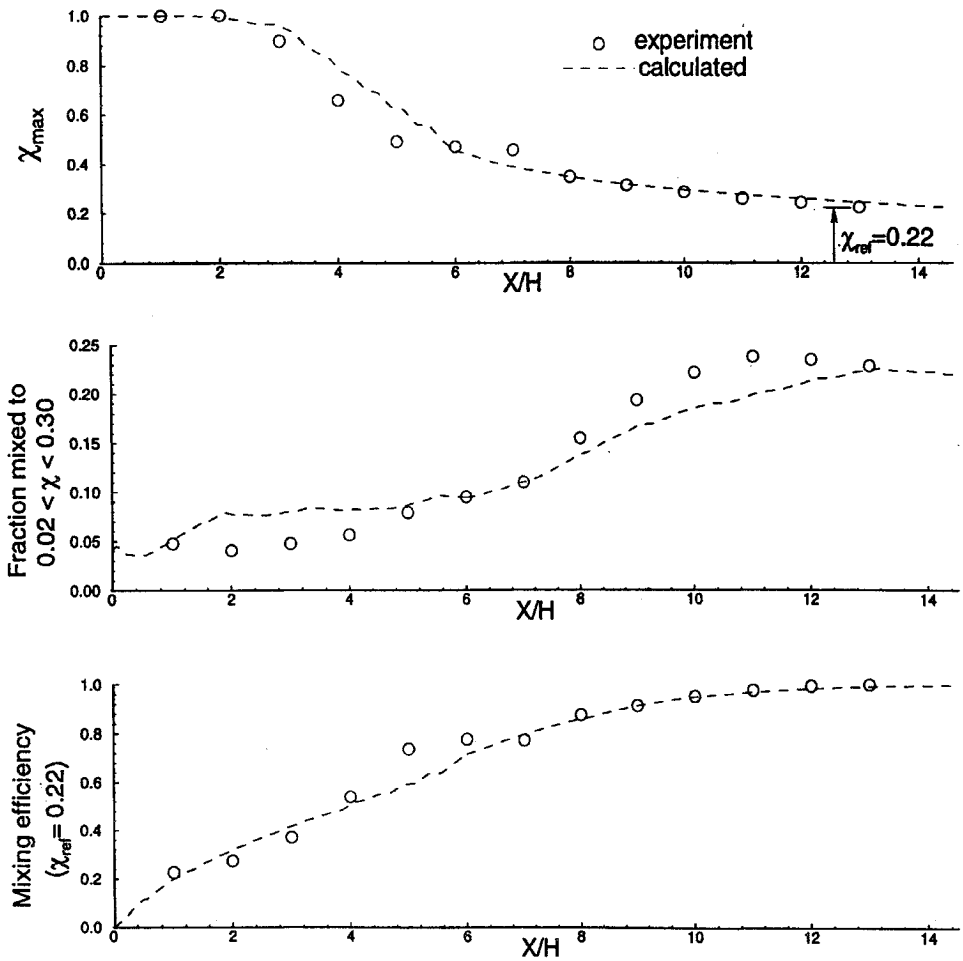

Fig. 11 Measures of mixing performance: decay of maximum injectant mole fraction, percentage area mixed, and mixing efficiency vs position downstream of the base of the ramp.

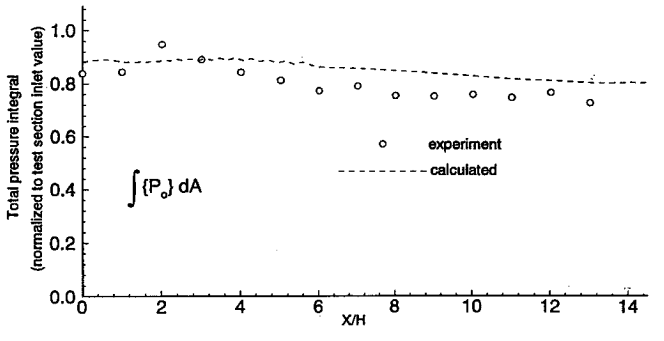

Fig. 12 Total pressure integral vs position downstream of the base of the ramp.

There is always a design tradeoff between increased mixing and flowfield losses, so that the ability to predict flowfield losses is a necessary step in validating a CFD code. To address this point, a plot showing integrated total pressure on crossflow planes is shown in Fig. 12. There has been some question in the literature as to whether this is the correct quantity to look at when evaluating losses. Several authors performing numerical studies have used other loss indicators, such as entropy increases, momentum flux changes, and thrust potential.[19] For the purposes herein of demonstrating that losses can be evaluated from the measured data set, the more traditional total pressure value will be used. The plots are normalized with the value extracted from a plane at the inlet to the test section before the ramp has had any influence on the flow. There is an initial 10–15% loss by $X/H = 2$ due to the strong shocks generated by the ramp and jet. Only about 5% additional loss occurs farther downstream due to the jet mixing and reflected shocks. The underprediction of losses seen in the calculated results is consistent with the slightly weaker shocks seen in the pressure results shown earlier.

In the first few planes (from $X/H = 0$ to about $X/H = 4$) the interpolation of the axial velocity from the coarsely spaced axial planes onto the crossflow planes may produce high errors since the lateral gradients in this near-field region are very large. This could explain the non-physical increase in total pressure seen between $X/H = 1$ and $X/H = 2$. There is a consistent underprediction of the total pressure losses in the numerical results after the initial few planes, where the total pressure integral falls above the experimental results by about 7%. Although the actual values are somewhat different, the trend in both curves is very similar at the downstream end where the interpolation of velocity between the seven measured planes is more accurate.

Conclusions

A complete three-dimensional flowfield mapping experiment was carried out in the flowfield of a supersonic unswept ramp fuel injector using planar laser-induced iodine fluorescence. Air, used as the simulated fuel, is injected at Mach 2.0 into a Mach 2.9 freestream. By fully automating the test setup, numerous planes of data were collected, and a data set that spans the entire test section was generated. The technique produces time-averaged measurements of pressure, temperature, velocity, and injectant mole fraction. The measurements allow any desired gasdynamic quantity to be determined on a three-dimensional grid, similar to the type of result generated by CFD simulations. The example planar results presented reveal both qualitative information about the features of the flowfield, as well as quantitative data that can be used to compare to other experimental methods or to validate numerical simulations. For all of the results presented, comparisons to a CFD calculation with the SPARK three-dimensional Navier–Stokes solver are made. Because of the completeness of the data set, global information about the flowfield, such as mass, momentum, and energy conservation checks, various mixing performance measures and flowfield losses could be determined. Measurement uncertainties in these global quantities are estimated to be about 2%, whereas the uncertainties in the individual gasdynamic parameters are estimated to be 5–8% for temperature, 4–10% for pressure, 10–20 m/s for velocity, and 2–3% for injectant mole fraction. Uncertainties are higher in regions close to walls due to high levels of scattered light from tunnel walls. These results demonstrate the level of consistency and accuracy possible with the PLIIF measurement technique. The ability to generate extensive data sets, such as the one presented here, demonstrates that the PLIIF technique can be used 1) to generate detailed test cases for the validation of CFD codes and 2) as an alternative to CFD for performing design studies and performance evaluation in complex compressible flowfields.

Acknowledgments

This work has been supported by the NASA Langley Research Center under Grant NAG-1-795 and NASA Graduate Student Researchers Program Grant NGT-50897, G. Burton Northam, technical monitor. The authors also acknowledge J. P. Drummond for providing the computer code and Cray CPU time used for the CFD simulation.

References

[1]Northam, G. B., Greenberg, I., and Byington, C. S., "Evaluation of Parallel Injection Configurations for Supersonic Combustion," AIAA Paper 89-2525, July 1989.

[2]Hartfield, R. J., Jr., Hollo, S. D., and McDaniel, J. C., "Experimental Investigation of a Supersonic Swept Ramp Injector Using Laser-Induced Iodine Fluorescence," *Journal of Propulsion and Power*, Vol. 10, No. 1, 1994, pp. 129–135.

[3]Waitz, I. A., Marble, F. E., and Zukoski, E. E., "An Investigation of a Contoured Wall Injector for Hypervelocity Mixing Augmentation," *AIAA Journal*, Vol. 31, No. 6, 1993, pp. 1014–1021.

[4]Riggins, D. W., Mekkes, G. L., McClinton, C. R., and Drummond, J. R., "A Numerical Study of Mixing Enhancement in a Supersonic Combustor," AIAA Paper 90-0203, Jan. 1990.

[5]Donohue, J. M., Haj-Hariri, H., and McDaniel, J. C., "Vorticity Generation Mechanisms in Parallel Injection Schemes for Supersonic Mixing," AIAA Paper 92-3286, July 1992.

[6]Donohue, J. M., McDaniel, J. C., and Haj-Hariri, H., "Experimental and Numerical Study of Swept Ramp Injection into a Supersonic Flowfield," *AIAA Journal*, Vol. 32, No. 9, 1994, pp. 1860–1867.

[7]McDaniel, J. C., Fletcher, D., Hartfield, R., and Hollo, S., "Staged Transverse Injection Into Mach 2 Flow Behind a Rearward-Facing Step: A 3-D Compressible Test Case for Hypersonic Combustor Code Validation," AIAA Paper 91-5071, Dec. 1991.

[8]Eklund, D. R., Fletcher, D. G., Hartfield, R. J., McDaniel, J. C., Northam, G. B., Dancey, C. L., and Wang, J. A., "A Computational/Experimental Investigation of Staged Normal Injection into a Mach 2 Flow," *AIAA Journal*, Vol. 37, No. 5, 1994, pp. 907–916.

[9]Drummond, J. P., "A Two Dimensional Numerical Simulation of a Supersonic, Chemically Reacting Mixing Layer," NASA TM-4055, Dec. 1988.

[10]Carpenter, M. H., "Three-Dimensional Computations of Cross-Flow Injection and Combustion in a Supersonic Flow," AIAA Paper 89-1870, June 1989.

[11]McDaniel, J. C., "Investigation of Laser-Induced Fluorescence for the Measurement of Density in Compressible Flows," Ph.D. Dissertation, Dept. of Aeronautics and Astronautics, Stanford Univ., Stanford, CA, 1982.

[12]Fletcher, D. G., "Spatially-Resolved, Nonintrusive Measurements in a Nonreacting Scramjet Combustor Using Laser-Induced Iodine Fluorescence," Ph.D. Dissertation, Dept. of Mechanical and Aerospace Engineering, Univ. of Virginia, Charlottesville, VA, Jan. 1989.

[13]Hartfield, R. J., "Planar Measurement of Flow Field Parameters in Nonreacting Supersonic Flows with Laser-Induced Iodine Fluorescence," Ph.D. Dissertation, Dept. of Mechanical Aerospace Engineering, Univ. of Virginia, Charlottesville, VA, May 1991.

[14]Hartfield, R. J., Jr., Hollo, S. D., and McDaniel, J. C., "A Unified Planar Measurement Technique for Compressible Flows Using Laser-Induced Iodine Fluorescence," *AIAA Journal*, Vol. 31, No. 3, 1993, pp. 483–490.

[15]Donohue, J. M., Victor, K. G., and McDaniel, J. C., "Computer Controlled Multi-Parameter Mapping of 3D Compressible Flowfields Using Planar Laser-Induced Iodine Fluorescence," AIAA Paper 93-0048, Jan. 1993.

[16]Donohue, J. M., "Experimental and Numerical Study of Ramp Injectors for Supersonic Fuel/Air Mixing," Ph.D. Dissertation, Dept. of Mechanical, Aerospace, and Nuclear Engineering, Univ., of Virginia, Charlottesville, VA, Jan. 1995.

[17]Nickol, C. L., "Unswept Ramp Fuel Injector Base Aspect Ratio Parametric Study in a Mach 2.9 Freestream," M.S. Thesis, Dept. of Mechanical and Aerospace Engineering, Univ. of Virginia, Charlottesville, VA, May 1994.

[18]Rogers, R. C., "Mixing of Hydrogen Injected from Multiple Injectors Normal to a Supersonic Airstream," NASA-TN-D 6476, Sept. 1971.

[19]Riggins, D. W., and McClinton, C. R., "Analysis of Losses in Supersonic Mixing and Reacting Flows," AIAA Paper 91-2266, June 1991.